UNIVERSITÄT AUGSBURG
Universitätsbibliothek

OPEN ACCESS
OPUS AUGSBURG

Oxygen feed membranes in autothermal steam-reformers –a robust temperature control

Jens Hüppmeier, Suelen Barg, Michael Baune, Dietmar Koch, Georg Grathwohl, Jorg Thöming

Angaben zur Veröffentlichung / Publication details:

Hüppmeier, Jens, Suelen Barg, Michael Baune, Dietmar Koch, Georg Grathwohl, and Jorg Thöming. 2010. "Oxygen feed membranes in autothermal steam-reformers –a robust temperature control." *Fuel* 89 (6): 1257–64. https://doi.org/10.1016/j.fuel.2009.09.023.

Nutzungsbedingungen / Terms of use:

CC BY-NC-ND 4.0

Dieses Dokument wird unter folgenden Bedingungen zur Verfügung gestellt: / This document is made available under these conditions:
CC-BY-NC-ND 4.0: Creative Commons: Namensnennung - Nicht kommerziell - Keine Bearbeitung
Weitere Informationen finden Sie unter: / For more information see:
https://creativecommons.org/licenses/by-nc-nd/4.0/deed.de

Oxygen feed membranes in autothermal steam-reformers – A robust temperature control

Jens Hüppmeier [a,*], Suelen Barg [b], Michael Baune [a], Dietmar Koch [b], Georg Grathwohl [b], Jorg Thöming [a]

[a] Center for Environmental Research and Sustainable Technology – UFT, University of Bremen, 28359 Bremen, Germany
[b] Ceramic Materials and Components – CERAMICS, University of Bremen, 28359 Bremen, Germany

1. Introduction

In conventional concepts for autothermal steam-reformers, the spatial temperature distribution is disadvantageous. The different reaction rates of the exothermic oxidation and endothermic reforming reactions lead to the problem of temperature hot-spots (Fig. 1), which can damage or even destroy the catalyst or other elements of the reformer. This is especially critical in the case when the required oxygen is premixed with the feed gas stream resulting in a high temperature peak at the entrance region [1–6]. Some typical temperature profiles for different experimental setups for methane as well as methanol autothermal reforming are shown in Fig. 1. These profiles indicate that the high temperature is located only in the first 20–30% of the reformer. After this peak, an almost equilibrium temperature is reached on a much lower level. Li et al. [1] came to the same results by observing the temperature profile with IR-thermography.

In the literature, some first attempts have been made to solve this hot-spot problem. The thermal coupling e.g. is one concept often used in micro reactors [4–8]. In these investigations, the different reaction zones were physically separated and thermally connected by a plate or the reactor wall. This reduces the temperature peak and allows a quick transport of the exothermically produced heat to the reforming site. Also a periodic reverse flow can be used for flattening the peak by using the heat capacity of the catalyst as heat storage [9,10]. Another concept is that the oxygen is not premixed to the feed gas but injected at different positions distributed over the length of the reformer. This leads to more but much smaller temperature peaks [2,3,11]. Extending this idea, we suggest a continuous injection with an oxygen flow rate varying over the reformer length. This approach includes open porous ceramic membranes that allow the adjustment of spatial oxygen flux distributions by means of spatially varying permeability (Fig. 2).

In contrast to the before mentioned concepts that focus on a reduction of the temperature peak only, our aim is to avoid this peak completely, i.e. we aspire to an isothermal behaviour of the autothermal steam-reformer. To achieve this with an open porous membrane, we lately performed an optimization procedure for identifying the best permeability distribution [12]. For a better understanding of this concept, we summarise this procedure in Section 1.2. The present work, however, concerns the realization of this concept and the purposeful designing and preparation of such a temperature control membrane.

Ceramic open porous membranes can be prepared by a low cost direct foaming method [13–15]. An alkane phase is emulsified in an aqueous inorganic powder suspension giving rise to a low alkane phase (LAPES) or high alkane phase emulsified suspensions (HAPES) depending on the dispersed phase content. In

* Corresponding author. Tel.: +49 421 218 6 33 86; fax: +49 421 218 82 97.
E-mail address: jhuepp@uni-bremen.de (J. Hüppmeier).

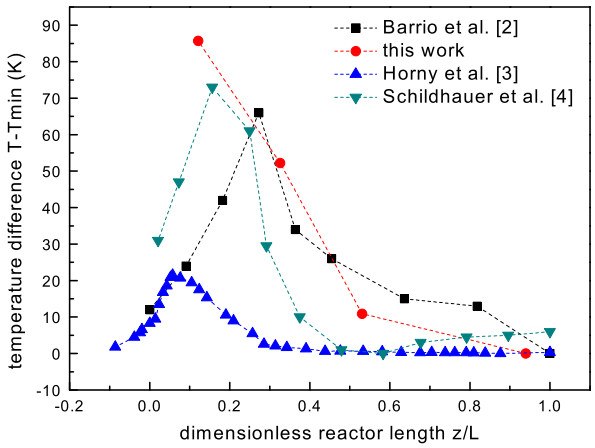

Fig. 1. Temperature peaks in the entrance region of conventional autothermal steam-reformers.

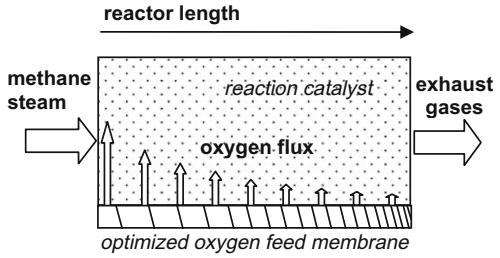

Fig. 2. Oxygen feed strategy for autothermal steam-reformers. The key element is an oxygen feed membrane with varying permeability over reactor length.

HAPES-based systems the porosity parameters of the emerging cellular structure can be easily controlled in the low micrometer scale by the adjustment of droplet size and concentration during emulsification. Given the versatility of the process, it can be easily adapted to different compositions resulting in mechanically stable parts of particularly tailored microstructural features with the possible formation of graded structures of self assembled open porous interfaces [15].

1.1. Previous work

Previous investigations [12] focused on a numerical optimization procedure of the membrane structure to achieve theoretically an isothermal behaviour of the adiabatic autothermal steam-reformer. Because the temperatures inside the reformer depend strongly on the local amount of oxygen, a key element is a system for controlling the air supply to the reformer. In contrast to normal control systems, we did not use the time as the independent variable but instead the location, z, along the length of the reformer (Fig. 3).

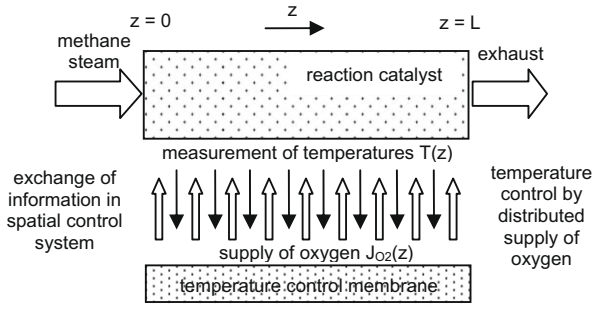

Fig. 3. Spatial control system consisting of the reformer, the temperature measurement on location z and a local supply of the oxygen controlled by a membrane.

During optimization by a digital controller, we calculated the temperature, $T(z)$, at each location z and compared it to the desired isothermal value T_{iso}. If the temperature were too low, the controller supplied more air, and if it were too high, it supplied less. We found a controller with proportional and differential characteristic (PD-controller) giving the best results for our system. In Fig. 4 the whole procedure is depicted. First, we built a "spatial control system", containing a one-dimensional steady-state model of the autothermal steam-reformer and a digital PD-controller (1). Then we tried to reach an isothermal distribution in the reformer (2) and extracted the therefore required oxygen flux distribution supplied by the controller (3). The last step was to transform the flow distribution to a membrane permeability distribution via Darcy's law (4).

The outcome of this investigation is shown in Fig. 5 and can be summarized with two important findings. First, some amount of oxygen must be premixed with the feed gases (in our case-study 11 %) in order to obtain an ignitable mixture in the entrance region and to start the catalytic reactions. Second, an oxygen flux is needed that decreases exponentially over the length of the reactor.

Consequently, the objective of this work is to validate experimentally the predicted isothermal behaviour of a reformer with a membrane oxygen distributer applying innovative HAPES-based oxygen feed membranes with designed permeability profiles.

2. Experimental setup

2.1. Autothermal steam-reformer

All the experiments were done with the setup described in Fig. 6. The three reactants for autothermal steam-reforming, namely methane, air and liquid water were supplied to the system via two mass flow controllers and a flow controlled syringe pump, respectively. The gases were preheated and the water vaporized and preheated by an external electric heater. Before entering this heater, the air mass flow was split via the adjustable valves V1 and V2. The stream through V1 is dedicated to flow through the membrane. The stream passing valve V2 is premixed with the other reactants methane and steam. The composition of the exhaust gases was measured by gas chromatography. The valve V3 served as a security valve. The reaction chamber and therefore the catalyst were of the size 66 × 20 × 18 mm. For measurement of the temperature profile inside the reformer, four thermocouples were located on the centerline of the catalyst. The distances of each thermocouple from the entrance were 8, 21.5, 35 and 62 mm. As catalyst, Pt-coated Al_2O_3-pallets of size 2 mm provided by Stonemill catalysts were used. In preliminary tests, this catalyst was found more stable against high temperature and temperature shocks than Ni-based catalysts.

The operation conditions for all experiments when it is not given explicitly can be found in Table 1. All tests were run with the same procedure; the reformer was heated up to a constant temperature of 550 °C and then the gas flow was started. The temperature measurement started after reaching a steady-state of the operation and was recorded for a minimum of 120 s to assure the constant values. In the same period, the output gas stream was sampled and measured by gas chromatography. By computer analysis, the conversion rate of methane defined by

$$X_{CH4} = \frac{\dot{n}_{inlet}^{CH4} - \dot{n}_{outlet}^{CH4}}{\dot{n}_{inlet}^{CH4}}, \qquad (1)$$

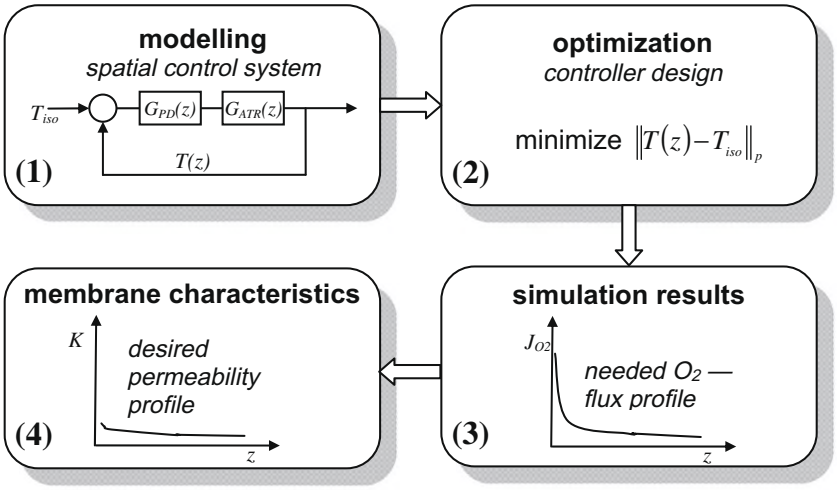

Fig. 4. Optimization procedure for an oxygen supply membrane to achieve an isothermal behaviour of the autothermal reformer. From building a model of the spatial control system (1) to designing the controller by simulations (2), to extracting the desired oxygen flux (3) leading to the desired permeability profile of the membrane (4).

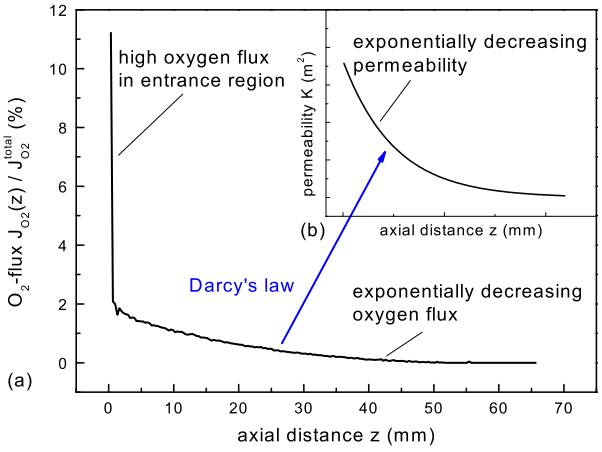

Fig. 5. Simulation results from the optimization procedure. The needed oxygen flux profile (a) can be expressed via Darcy's law as a permeability profile (b) of an open porous membrane.

the selectivity of hydrogen defined by

$$S_{H2} = \frac{\dot{n}^{H2}_{outlet}}{\dot{n}^{CH4}_{inlet} - \dot{n}^{CH4}_{outlet}} \tag{2}$$

and the selectivity of CO defined by

Table 1
Operation conditions for the experiments.

Total mass flux (10^{-5} kg/s)	5
O_2/CH_4-ratio	0.379
H_2O/CH_4-ratio	1.621
Preheated gas temperature (°C)	550

$$S_{CO} = \frac{\dot{n}^{CO}_{outlet}}{\dot{n}^{CH4}_{inlet} - \dot{n}^{CH4}_{outlet}} \tag{3}$$

was carried out from these samples.

2.2. Oxygen feed membranes

Oxygen feed open porous alumina membranes with varying cell size distributions are prepared. Membranes composed of single cell size as well as a combination of membranes with varying cell size distribution are tested for the realization of simulated optimal permeability distributions.

2.2.1. Membrane preparation

For the realization of the oxygen feed membranes, the first step is the preparation of a high alkane phase emulsified alumina suspension (alumina-HAPES). For this, initially a stabilized alumina

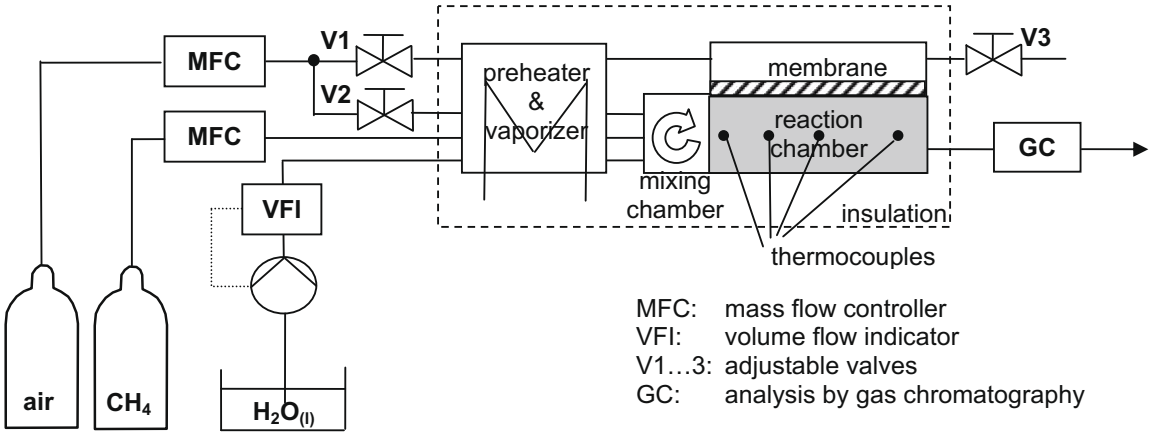

Fig. 6. Experimental setup for the membrane tests consisting of the autothermal reformer, a preheater and vaporizer and the control and measurement equipment.

powder suspension was prepared by the slow addition of dry alumina powder (Alcoa CT 3000 SG) with an average particle diameter (d_{50}) of 500 nm and a specific surface area of 7.5 m^2/g into deionised water containing Dolapix CE-64 (0.74 wt.% related to alumina) as negatively charged electrosteric dispersion [16]. Dispersion and homogenization was carried out in a laboratory mixer (Dispermat LC, VMA Getzmann GmbH) at a mixing velocity of 2500 rpm for 20 min. The particle content in the suspensions was set as 42 vol.%. Afterwards the alumina suspensions were subjected to de-aeration to remove undesired entrapped bubbles under reduced pressure (5 kPa). Alumina-HAPES were prepared by adding 70 vol.% decane ($C_{10}H_{22}$) from Fluka and sodium lauryl sulphate (SLS) (BASF, Lutensid AS 2230) as anionic surfactant (between 0.11 and 0.22 vol.%, depending on the employed stirring rate). To ensure the stability of the system, the addition of this surfactant must take into account the zeta potential and isoelectric point (IEP) of the alumina suspension. Therefore, it is used under alkaline conditions (pH 9.5) where the strong negative zeta potential is provided by the dispersion agent [13].

The alkane droplet size is very important to be controlled regarding its strong influence on the cell and window size of the emerging open porous structures. The droplet size was controlled by the application of different stirring rates (from 800 to 2500 rpm) during 2.5 min of emulsification. Emulsification is undertaken under reduced pressure (10 kPa) at room temperature to avoid the abundant incorporation of air bubbles and also preventing evaporation of decane which has a vapor pressure of 0.19 kPa at 25 °C.

Afterwards, the alumina-HAPES of defined droplets size are cast into a stationary PVC mold with the subsequent movement of a doctor blade along the surface of the filled mold that ensures the removal of excess HAPES and provides precise shaping of the green foam keeping the upper surface opened to the atmosphere. The consolidation of the molded HAPES proceeds under limited foaming by a minimal expansion of the alkane droplets and drying of the aqueous solvent. Complete drying of the foams is achieved at room temperature during 3 days. After de-molding, the alumina membranes are sintered at 1550 °C for 2 h with heating and cooling rates of 2 K/min.

2.2.2. Membrane characterization

The morphology and microstructure of the sintered materials were evaluated from micrographs taken by Scanning Electron Microscopy, SEM (Camscan 24). Cell sizes were measured from planar sections with the linear intercept method (Linear Intercept, TU Darmstadt). The average cell size d_{50} was determined from the cumulative cell size distribution curves of 3 pictures taken from different regions of the sample. The window size distribution was measured by Hg-Intrusion (Pascal 140/440, CE Instruments). The total and open porosity of the materials was calculated by the Archimedes method considering three different weights of the specimen: m_1 (the dry specimen weight), m_2 (weight of the specimen under water), and m_3 (weight of the wet specimen).

Gas permeability was determined measuring the gas mass flow rate through the materials for controlled differential pressures ranging from 0 to 1 bar (Topas PSM 165). Permeability constants K_1 and K_2 were obtained from Forchheimer's equation, expressed for flow of compressible fluids (Eq. (1)) fitting the experimental data by a standard least squares method [17,18].

$$\frac{(p_i^2 - p_0^2)}{2lp_0} = \frac{\mu}{K_1}u + \frac{\rho}{K_2}u^2 \tag{4}$$

where p_i and p_0 denote, respectively, the pressure of incoming gas flow before and after passing through the membrane, l is the membrane thickness (2.4–3.8 mm), ρ is the gas density (1.19 kg/m^3) and μ the gas viscosity (1.83×10^{-5} Pa s), which are calculated from reference conditions of $p_0 = 1010$ mbar and room temperature of 295 K. The superficial velocity of the fluid ($u = \dot{V}/A$) was calculated from the volumetric flow rate $\dot{V}$ at the mentioned reference conditions and free flow area, A, of 0.95 cm^2.

Uniaxial compressive strength tests were performed in a hydraulic mechanical testing machine (Zwick Model Germany), applying a cross-head speed of 1.3 mm/min and a compressive load cell of 5000 N (following ASTM C133-94 standard). For each parameter investigated, 20 to 30 specimens measuring $10 \times 10 \times 10$ mm^3 were tested. The compressive strengths are calculated from the maximal strength in the compressive stress–strain curves.

3. Experimental results

3.1. Oxygen feed membranes

3.1.1. Qualitative results

The microstructures of sintered alumina membranes produced from HAPES emulsified under 800, 1500 and 2500 rpm are represented in Fig. 7. The materials are characterized by highly interconnected cells, which are uniformly distributed throughout the sample. The emulsification stirring rate controls the droplet size and consequently the cell size distribution. With increasing stirring rate, the average cell size decreases and narrower cell size distributions are realised (Fig. 7c). The connections between alkane droplets in HAPES and the bubbles emerging from this phase are characterized by thin films (lamellae). During evaporation and drying, these bubbles open up, partially providing thereby windows between adjacent cells. The windows size is proportional to the cell size and decreases like the cell size with the increasing stirring rate. In spite of the strongly varying microstructure, the total porosity was effectively kept between 77.6% and 78.8% by keeping the HAPES alkane content constant. As a consequence of the fixed total porosity, smaller cell sizes turn out as a higher cell concentration, and consequently higher surface areas are generated. Thus, larger celled structures present thicker struts (Fig. 7).

3.1.2. Quantitative results

The quantitative results providing the physical and mechanical characterization are presented in Table 2 as being influenced by the emulsification stirring rate. A reduction of the average cell size (d_{50}) from 20 to 6 μm, the average window size from 13 to 4 μm and the strut thickness from 14 to 3 μm is measured when HAPES is emulsified under 800 and 2500 rpm, respectively. Furthermore, large cell size distributions (resulting from emulsification under 800 rpm) can lead occasionally to isolated small pores enclosed in the struts (Fig. 7) resulting in reduction of open porosity (71%). The materials are characterized by excellent compressive strengths from 17.3 to 31.1 MPa. As proposed by Gibson and Ashby, the compressive strength tends to increase with the the strut thickness to cell size ratio (t/l) increase [19]. However, alumina foams with the highest t/l (produced under the lowest stirring rate of 800 rpm) presented a lower compressive strength (29.5 MPa) than expected which may be the effect of the broad cell size distribution and the presence of closed pores inside the struts.

The permeability of porous materials is strongly influenced by the porosity parameters and the processing route. Consequently, many empirical equations are available for the prediction of permeability in porous media. In particular, Richardson et al. [20] proposed that the permeability coefficients depend on the volumetric surface, S_v. In this model, the permeability coefficients K_1 and K_2 are estimated as follow:

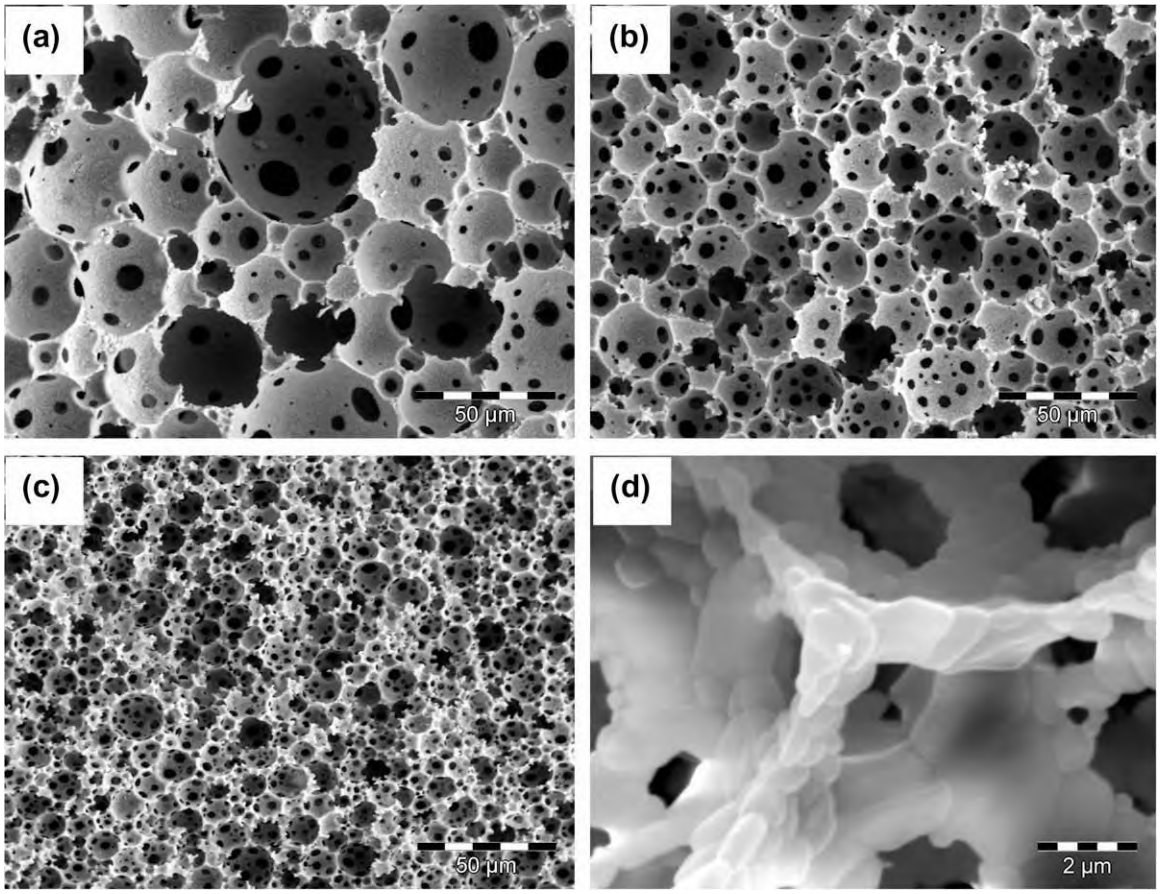

Fig. 7. Microstructure of sintered alumina foams produced from HAPES containing 42 vol.% particle content emulsified under (a) 800 rpm, (b) 1500 rpm, (c) and (d) 2500 rpm. In (d) dense struts composed by a single layer of alumina particles are represented [13].

Table 2
Summary of physical and mechanical characterization of alumina membranes.

Stirring velocitiy ω (rpm)	Cell size l_{50} (μm)	Window size d_{50} (μm)	Strut thickness t_{50} (μm)	Strut thickness/cell size t_{50}/l_{50} (μm)	Total porosity ε_{total} (%)	Open porosity ε_{open} (%)	Permeability coefficients		Compressive strength σ (MPa)
							K_1 (10^{-12} m^2)	K_2 (10^{-6} m)	
800	20.7 ± 1.2	12.8 ± 0.8	13.5 ± 2	0.65	77.8 ± 0.6	71.0 ± 1.7	3.79	2.31	29.4 ± 5.5
1500	9.0 ± 0.54	5.9 ± 0.3	5.5 ± 0.1	0.60	78.8 ± 0.2	78.5 ± 0.6	1.24	1.30	31.1 ± 7.2
1800	6.2 ± 0.52	–	3.6 ± 0.1	0.57	78.8 ± 0.05	78.1 ± 0.2	0.98	1.63	25.9 ± 5.5
2500	5.4 ± 0.02	3.5 ± 0.05	2.7 ± 0.04	0.49	77.6 ± 0.3	77.2 ± 0.1	0.39	0.2	17.32 ± 6.1

$$K_1 = \frac{\varepsilon^3}{\alpha S_v^2 (1-\varepsilon)^2} \quad (5)$$

$$K_2 = \frac{\varepsilon^3}{\beta S_v (1-\varepsilon)} \quad (6)$$

The parameters α and β depend on the porosity ε and on the pore sizes d_p. The model derived by Richardson was estimated with Replica-foams that had pore sizes in the range of 0.3–1.7 mm, what is far from the range of pore sizes of our membrane what is about 5–20 μm. This results in a modification of the Richardson model with the same model structure but slightly different coefficients. The following correlations based on the Richardson model can be used to describe the dependence of permeability with the porosity parameters:

$$\alpha = 11.130 \times 10^2 d_p^{0.5104} (1-\varepsilon)^{-0.1058} \quad (7)$$

$$\beta = 3.8127 \times 10^{-4} d_p^{-0.7328} (1-\varepsilon)^{0.0815} \quad (8)$$

The membrane permeability constants K_1 and K_2 as well as the values predicted by the modified Richardson model as a function of average cell size are represented in Fig. 8. The permeability constants tend to decrease with the decrease in cell size as proposed by the modified Richardson model. The membranes with controlled cell structures presented permeability constants varying between 3.8×10^{-12} and 3.9×10^{-13} m^2 for K_1, and 2.3×10^{-6} and 2×10^{-7} m for K_2.

By this way the permeability of the membranes could be efficiently designed by the control of the shear stresses in the droplet surface during emulsification. The potential to produce crack-free open porous ceramic membranes with controllable porosity parameters is a manifestation of the high structural stability of HAPES which resists the capillary stresses during consolidation, with a minimum expansion of the pore formers.

3.1.3. Membranes with staged permeabilities

With stirring rates 800, 1500, 1800 and 2500 rpm, we obtained four membranes with different but constant permeability. As a representative for the Darcian permeability, K_1 is shown versus the axial distance z of the reformer as thin small dashed black lines (Fig. 9). Because it was not possible to produce a membrane with

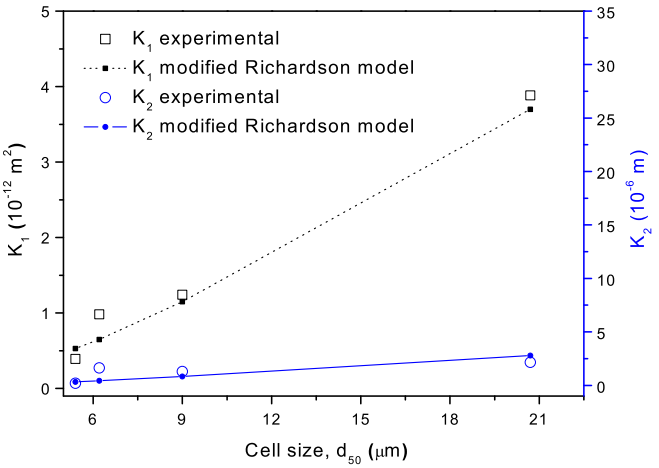

Fig. 8. Comparison between experimental permeability coefficients K_1 and K_2 and values predicted by modified Richardson model (Eq. (2)), utilizing open porosity (ε_{open}) and average cell size (l_{50}) (Table 2).

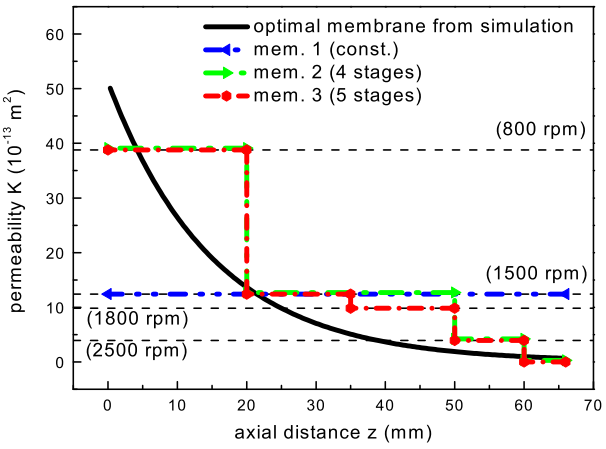

Fig. 9. Desired permeability profile over the length of the reformer compared to real membranes and a combination of these membranes.

the calculated permeability distribution directly (solid black line), we approached stepwise the optimum profile by cutting the four membranes and combine the sliced pieces together by gluing them with high temperature cement. Two membranes with staged permeabilities were produced this way, a 4-stage membrane represented by the yellow dashed line and a 5-stage membrane shown in Fig. 9 as a dash-dotted line. In Section 3.2 we compare the two membranes with staged permeabilities as well as a membrane with single constant permeability (1500 rpm) with the normal operation without oxygen feed membrane.

3.2. Membrane performance

In Fig. 10 the temperature profiles are shown for the tested temperature control membranes compared to the operation without a membrane. The operating conditions were all the same for these experiments. According to our simulation results, we added a small amount of the oxygen to the feed gases in order to obtain the target temperature in the entrance region. The amounts were 5.2% for the membrane with the constant permeability and 6.5% for the graded one.

For the membrane with the constant permeability marked with the circles, we can avoid the hot-spot in the entrance region. How-

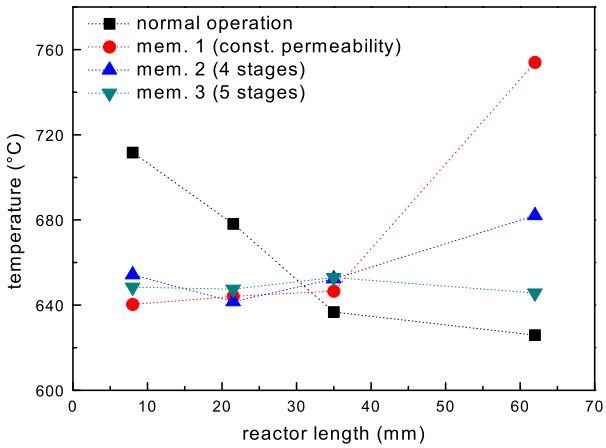

Fig. 10. Temperature profiles along the length of the reformer using different temperature control membranes at their optimal operation points.

ever, another significant temperature increase now appears and is located near the reactor exit. This is due to the continuous constant feed of oxygen over the length of the reformer providing excess oxygen. This temperature peak is even higher than the initial one for the case without a membrane. Also for the first membrane with 4 permeability stages we still found a small enhancement of temperature at the end of the reformer. Accordingly, we introduced a fifth stage and with this membrane we obtained an almost isothermal temperature profile. The absolute deviation of the temperature to a mean value of 650 °C is less than 5 K.

Furthermore, it is necessary to ensure that the operation with the porous membrane produces at least as much hydrogen as that of the conventional operation. We compared the conversion rate of methane (Eq. (1)), the selectivity of hydrogen (Eq. (2)) and the selectivity of CO (Eq. (3)) for the reactor configurations with different membranes and without.

The results are shown in Fig. 11 and for the conversion rate the values are similar. The deviations were less than 3% for the 5-stage membrane. Also the results for the selectivities are similar to the conventional operation. Only in the case of the membrane with constant permeability are the selectivities significantly lower. This is because of the high concentration of oxygen at the end of the reformer. With more oxygen we support the oxidation reactions and produce more H_2O and CO_2 rather than hydrogen and CO. This

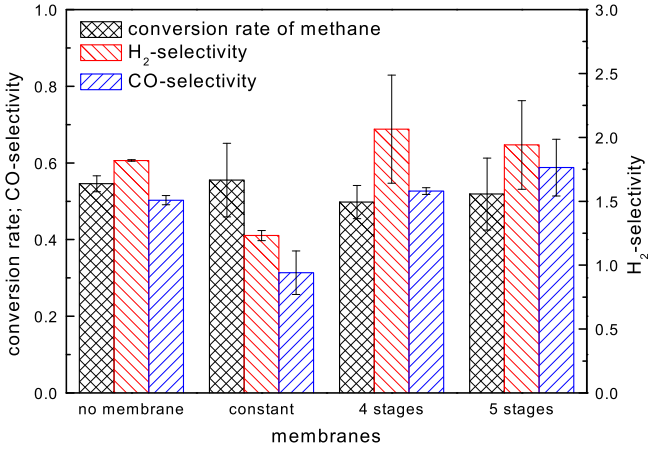

Fig. 11. Conversion rates and selectivities using different temperature control membranes at their optimal operation points. Error bars indicate the standard deviation obtained from experiments.

effect can also be seen in the temperature peak in Fig. 10. The selectivities for the staged membranes instead were about the same as with the conventional one or at least with respect to the high standard deviation values a little bit higher.

We also investigated the effect of premixing different amounts of oxygen to the feed gas using the best membrane, the one with 5 permeability stages. According to our simulation results, in the entrance region a high supply of oxygen is needed to start the partial oxidation reaction. This can not be achieved only by a membrane. Instead, by adjusting the valves V1 and V2 (Fig. 6) we varied the amount of premixed oxygen.

What can be seen from Fig. 12 is that the amount of premixed oxygen has a strong influence on the temperature in the entrance region. The influence on the total temperatures in the interior of the reformer is also detectable but not that significant. For the membrane No. 3, the best one, we found an optimum of 6.5% oxygen premixed to feed gases, which is 5% below the predicted value. This difference can be explained by a heat transfer, which was better in the experimental set-up compared to the assumptions made for the simulation. This finding is in accord with our observation that the measured temperature peak is not as sharp as the calculated one [12].

Again, we investigated also the conversion rates and selectivities for these operations. The results in Fig. 13 indicate that the effect of premixed oxygen on these quantities is quite low, as well. Only without premixing are the values smaller compared to the other ones. According to the low temperatures measured this is due to the relatively low absolute amount of heat produced, which in turn limits steam-reforming (Fig. 12).

Beside the requirements of conversion rate and selectivity in the membrane operation, it was another question in our work to estimate, what energy loss is caused by using such a membrane. Meaning that we need additional energy to press the air through the membrane instead of premixing. The relevant value here is of course the pressure loss of the membrane which was under 0.8 bar for all used membranes and our ranges of operations (Table 1). This means that we had an energy loss of approximately 90 kJ per kg reformate. The calculations were done with respect to the density of air at 550 °C which was 0.373 kg/m^3 and assuming that we need 0.41 kg of air per kg reformate. This leads to the fact that the energy loss caused by the pressure loss of the membrane is <1% of the reformate's higher heating value (HHV). This was about 25 MJ/kg for a typical output of our reformer (~12 wt.% H_2, ~4 wt.% CO, ~11 wt.% CH_4).

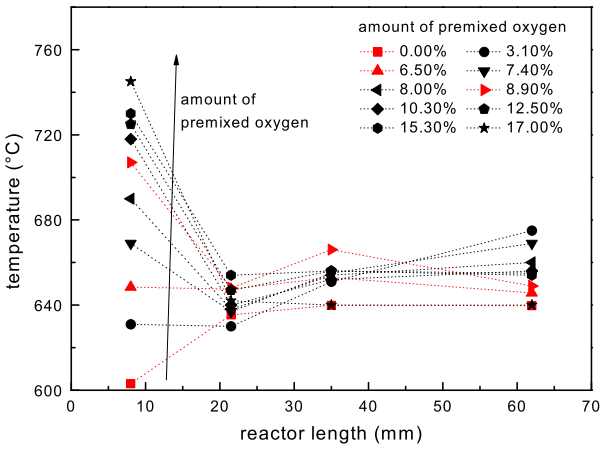

Fig. 12. Temperature profiles along the length of the reformer using the graded temperature control membrane with different amounts of oxygen added to the feed gases.

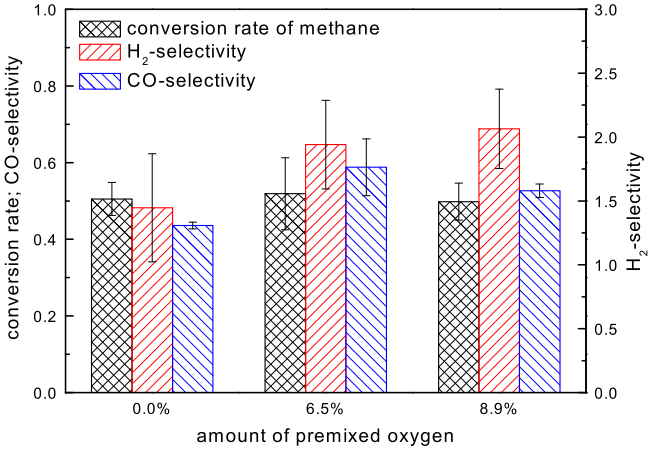

Fig. 13. Conversion rates and selectivities using the graded temperature control membrane with different amounts of oxygen added to the feed gases. Error bars indicate the standard deviation obtained from experiments.

4. Conclusions

Presented in this paper is the design, production and testing of an innovative oxygen feed membrane that allows almost isothermal operation in conventional small-scale autothermal steam-reformers, thereby avoiding the initial temperature peak that is well known for such units.

For a successful application it is of high importance that membrane parameters fit precisely to the demand calculated by means of a numerical optimization. The processing route based on HAPES leads to highly open porous ceramic membranes (open porosity between 71% and 78%, total porosity of 78%) with excellent mechanical properties due to the defect-free build up of the struts as well as designable permeability which could be correlated with the porosity parameters by the modified Richardson model.

These materials are used in a staged form to achieve the permeability profile calculated by an optimization procedure. As a consequence of our experimental results, it can be stated that the membrane with multi-staged permeabilities leads to almost isothermal conditions without losing the efficiency of the normal operation with respect to conversion rate and syngas selectivity. Also, the conclusion from our simulations, that a small amount of oxygen needs to be premixed to the feed gases, was confirmed in our experiments.

All findings presented here refer to a lab scale unit. However, up-scaling of this approach should be possible using tubular concepts. In case of reaction tubes with diameters in the centimeter range the tube could be the oxygen feed membrane, whereas for reaction tubes with several meters in diameter a number of small oxygen feed membrane tubes could be distributed equally over the cross section.

For up-scaling two more aspects must be considered. First, for the different applications we must find a better way for graded manufacturing of the membranes since the used cut and glue method is not practicable in every case. The foaming process is dedicated to be here the most practicable way since there are already some experiences with graded structures [21,22]. Second, we have to estimate the total operating range of such a membrane. The described optimization procedure was done for a specific set of space velocity, oxygen to carbon and steam to carbon ratio. What happens with the temperature distribution when operation conditions significantly change? Another aspect of the operating range is the long-term stability of those membranes at high temperatures. Although we do not expect problems with the highly temperature

stable Al_2O_3-membranes, this aspect must be assured before practical up-scaling.

Acknowledgements

The funding of the research project by the Deutsche Forschungsgemeinschaft through the Research Training Group "PoreNet" is gratefully acknowledged. Especially, we thank Marcus Vinicius Silveira for helping with the experimental work and Peter Behrend for the analysis of the gas samples by gas chromatography.

References

[1] Li B, Maruyama K, Nurunnabi M, Kunimori K, Tomishige K. Temperature profiles of alumina-supported noble metal catalysts in autothermal reforming of methane. Appl Catal A: Gen 2004;275:157–72.
[2] Barrio VL, Schaub G, Rohde M, Rabe S, Vogel F, Cambra JF, Arias PL, Güemez MB. Reactor modeling to simulate catalytic partial oxidation and steam reforming of methane. Comparison of temperature profiles and strategies for hot spot minimization. Int J Hydrogen Energy 2006. doi:10.1016/j.ijhydene.2006.10.022.
[3] Dutta S, Wright HA. Synthesis gas process comprising partial oxidation using controlled and optimized temperature profiles. US Patent Application Publication US 2006/0029539 A1, February 9, 2006 and US Patent 7,261,751 B2, August 28, 2007.
[4] Taki M, Mizuno S, Ozaki T, Kawahara T, Kinoshita K, Negishi Y. Fuel reformer divice, US Patent 6,887,286 B1, May 3, 2005.
[5] Horny C, Renken A, Kiwi-Minsker L. Compact string reactor for autothermal hydrogen production. Catal Today 2007;120:45–53.
[6] Schildhauer TJ, Geissler K. Reactor concept for improved heat integration in autothermal methanol reforming. Int J Hydrogen Energy 2007;32:1806–10.
[7] Kaisare NS, Deshmukh SR, Vlachos DG. Chem Eng Sci 2008;63:1098–116.
[8] Fazeli A, Behnam M. CFD Modeling of methane autothermal reforming in a catalytic microreactor. Int J Chem Eng 2007;5 [Article A93].
[9] Kaisare NS, Lee JH, Fedorov AG. Hydrogen generation in a reverse-flow microreactor. Part 1. Model formulation and scaling. AIChE J 2005;51(8):2254–64.
[10] Kaisare NS, Lee JH, Fedorov AG. Hydrogen generation in a reverse-flow microreactor. Part 2. Simulation and analysis. AIChE J 2005;51(8):2265–72.
[11] Tiemersma TP, Patil CS, van Sint Annaland M, Kuipers JAM. Modelling of packed bed membrane reactors for autothermal production of ultrapure hydrogen. Chem Eng Sci 2006;61:1602–16.
[12] Hüppmeier J, Baune M, Thöming J. Interactions between reaction kinetics in ATR-reactors and transport mechanisms in functional ceramic membranes: a simulation approach. Chem Eng J 2008;142:225–38.
[13] Barg S, Soltmann C, Andrade M, Koch D, Grathwohl G. Cellular ceramics by direct foaming of emulsified ceramic powder suspensions. J Am Ceramic Soc 2008;91(9):2823–9.
[14] Barg S, de Moraes EG, Koch D, Grathwohl G. New cellular ceramics from high alkane phase emulsified suspensions (HAPES). J Euro Ceramic Soc 2009;29(12):2439–46.
[15] Barg S, Koch D, Grathwohl G. Processing and properties of graded ceramic filters. J Am Ceramic Soc 2009; doi:10.1111/j.1551-2916.2009.03301.x.
[16] Schramm LL. Emulsions, foams and suspensions. Fundamentals and applications. John Wiley & Sons Inc.; 2006.
[17] Acchar W, Ramalho EG, Souza FBM, Torquato WL, Rodrigues VP, Innocentini MDM. Characterization of cellular ceramics for high-temperature applications. J Mater Sci 2008;43:6556–61.
[18] Innocentini MDM, Rodrigues VP, Romano RCO, Pileggi RG, Silva GMC, Coury JR. Permeability optimization performance evaluation of hot aerosol filters made using foam incorporated alumina suspension. J Hazardous Mater 2009;162(1):212–21.
[19] Gibson LJ, Ashby MF. Cellular solids: structure and properties. Cambridge: Cambridge University Press; 1997.
[20] Richardson JT, Peng Y, Remue D. Properties of ceramic foam catalyst supports: pressure drop. Appl Catal A: Gen 2000;204:19–32.
[21] Corbin SF, Zhao-Jie X, Henein H, Apte PS. Functionally graded metal/ceramic composites by tape casting, lamination and infiltration. Mater Sci Eng: A 1999;262:192–203.
[22] Zeschky J, Hofner T, Arnold C, Weissmann R, Bahloul-Hourlier D, Scheffler M, et al. Polysilsesquioxane derived ceramic foams with gradient porosity. Acta Mater 2005;53(4):927–37.